

DOUBLE INVERTED PENDULUM MODEL OF REACTIVE HUMAN STANCE CONTROL

Georg Hettich, Luminous Fennell and Thomas Mergner

Neurology, University of Freiburg,

Breisacher Str. 64, 79106 Freiburg, Germany

e-mail: georg.hettich@uniklinik-freiburg.de, mstrlu@gmx.net,

mergner@uni-freiburg.de

Keywords: Human Stance, Balancing, External Disturbances, Foot Support Tilt, Sensory Feedback Control Model, Double Inverted Pendulum Biomechanics.

Abstract: When maintaining equilibrium in upright stance, humans use sensory feedback control to cope with unforeseen external disturbances such as support surface motion, this despite biological ‘complications’ such as noisy and inaccurate sensor signals and considerable neural, motor, and processing time delays. The control method they use apparently differs from established methods one normally finds in technical fields. System identification recently led us design a control model that we currently test in our laboratory. The tests include hardware-in-the-loop simulations after the model’s embodiment into a robot. The model is called *disturbance estimation and compensation (DEC)* model. Disturbance estimation is performed by on-line *multisensory* interactions using joint angle, joint torque, and *vestibular* cues. For disturbance compensation, the method of direct disturbance rejection is used (“Störgrössenaufschaltung”). So far, biomechanics of a single inverted pendulum (SIP) were applied. Here we extend the DEC concept to the control of a double inverted pendulum (DIP; moving links: trunk on hip joint and legs on ankle joints). The aim is that the model copes in addition with inter-link torques and still describes human experimental data. As concerns the inter-link torque arising during leg motion in the hip joint (support base of the outer link, the trunk), it is already covered by the DEC concept we so far used for the SIP. The inter-link torque arising from trunk motion in the ankle joint is largely neutralized by the concept’s whole-body COM control through the ankle joint (due to the fact that body geometry and thus COM location changes with the inter-link motion). Experimentally, we applied pseudorandom support surface tilt stimuli in the sagittal plane to healthy human subjects who were standing with eyes closed on a motion platform (frequency range, 0.16 – 2.2 Hz). Angular excursions of trunk, leg, and whole-body COM (center of mass) with respect to the space vertical as well as COP (center of pressure) shifts were recorded and analyzed. The human data was compared to corresponding model and robot simulation data. The human findings were well described by the model and robot simulations. This shows that the DIP biomechanics of human reactive stance can be controlled using a purely sensor-based control.

1 INTRODUCTION

Maintaining upright biped stance is an important skill of humans for many activities of everyday life. Research that tried to formally describe this control often applied sagittal-plane single inverted pendulum (SIP) biomechanics with ankle joint actuation [1,2]. Such SIP models have successfully been used to describe human responses to external disturbances. Some of these SIP based models use continuous sensory feedback control with realistic neural time delays (e.g. [3]). However, humans often involve in addition to the ankle joints also the hip joints. Thereby they improve their balancing, increasing its flexibility in face of the multitude of external disturbance scenarios and its robustness in terms of fail safe. To better understand these skills, it is desirable to use double inverted pendulum (DIP) biomechanics in the modeling.

In human experiments, balancing using almost exclusively the ankle joint is called the ‘ankle strategy’, while involving in addition considerably the hip joint is called the ‘hip strategy’ [4,5]. Contributions from knee joints are known to be small [4,6]. They produce mainly vertical body acceleration, while most of the balancing deals with compensation of the horizontal accelerations of the body’s COM, which may lead to lift-off of heels or toes [7]. Human studies on the role of the ‘hip strategy’ emphasized different aspects, such as biomechanical factors (e.g. restriction of foot support base [5,8]), disturbance speed (fast speed favoring hip strategy [9] and slow speed favoring ankle strategy [5], or sensory restrictions through disease or age (see [10]). Approaches that focused more on biomechanics considered mainly other aspects, such as minimization of effort ([7,11]; less effort with hip strategy), specific minimization of inter-link torque effects [4], and the effect of movement synergies [12].

In some sensory feedback control models, it is assumed that multisensory integration makes a major contribution, this especially in view of the human system’s flexibility and robustness. In mainly engineering modeling approaches [13,14] automatic adjustments to environmental changes are performed by multisensory integration centers involving Kalman filters and efference copy. A recent neurological approach from our laboratory, in contrast, used a model that builds solely on sensory signals and their interactions for this purpose [15,16]. In software as well as hardware-in-the-loop (robot) simulations, the model was able to mimic human balancing across a variety of experimental conditions. However, the model uses SIP biomechanics. Here, we extend it to DIP biomechanics and compare software and hardware simulation results with corresponding human data.

In the following, only responses to external disturbances are considered, while ‘quiet stance’ remains unconsidered. In chapter 2, we describe our control model. In chapter 3, we introduce the DIP and its control. In chapter 4, we present results from model simulations, human experiments, and robot experiments performed in the human testbed (posture control laboratory), before presenting Discussion and Conclusions (5). The robot experiments are viewed here as a ‘proof of principle’, meaning that the software model, originally stemming from experimental identification of the human control system, is re-embodied into noisy and inaccurate real world environment.

2 DISTURBANCE ESTIMATION AND COMPENSATION (DEC) CONCEPT

Human balancing upon external disturbances can be modeled by continuous sensory feedback control of a SIP using a PID controller (*proportional, integral, derivative*), this despite loop time delays of 100 - 200 ms [3,17]. Several sensors are known to be involved: joint angle and joint torque proprioception, vestibular, and visual ([10]; the visual contribution will not be considered here). Human flexibility in face of considerably varying stimulus magnitudes and disturbance scenarios has been attributed to sensory reweightings. Different ways of

reweighting have been considered (see 1). Our model, based solely on inter-sensory interactions [15,16], proceeds from psychophysical work on self-motion perception. This suggested novel concepts of sensors and their interactions: (a) ‘Sensor concept’. The sensors integrate information from several sensory transducers and output measures of the here relevant kinematic and kinetic variables (e.g. joint angular velocity). (b) ‘Meta level concept’. A level of inter-sensory interactions is interleaved between sensor signals and feedback. At this level, the external events are reconstructed in terms of disturbance estimates.

The model assumes that four external disturbances are essential for biped balancing: (1) support surface tilt, (2) support surface translational acceleration, (3) field forces such as gravity, and (4) contact forces such as a push or pull having impact on the body (this disturbance and the joint torque cues that are required for its estimation will not be considered here). The disturbance estimates are used for disturbance compensation in a feedback control using the method of ‘Störgrössenaufschaltung’ (direct disturbance rejection through compensation injection). The disturbance estimation and compensation model (DEC model) accurately simulated the human experimental data we obtained so far (recent overview, [18]).

The DEC control method is schematically depicted in Fig. (1). Receiving a voluntary (‘pro-active’) set point signal and proprioceptive feedback information, a neural controller (C) commands the plant. External disturbances affecting the plant are internally reconstructed through sensors. Their estimates are directly used for disturbance compensation. This can occur either *after* the controller at the level of joint torque (not shown) or *before* the controller in terms of angles in joint or space coordinates (shown in Fig. 1). In view of considerable time delays in the loop, feedback of angular position tends to be advantageous for control stability compared to torque feedback.

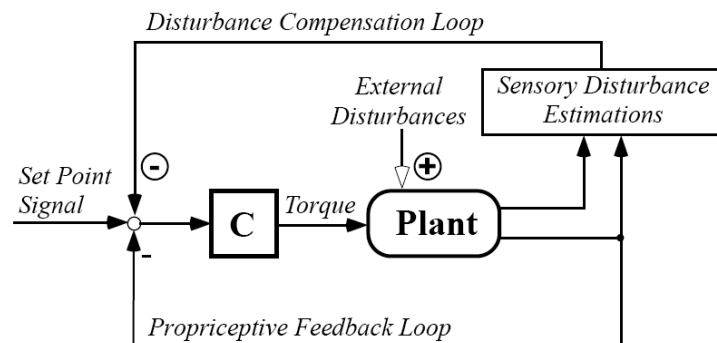


Figure 1: Disturbance Estimation and Compensation (DEC) method. C, neural controller. Actuator omitted, assumed to perform ideally in the present context. Also intrinsic muscle stiffness and viscosity effects (taken to be 15 % of reflexive values) are not shown.

The DEC model uses position (angle) feedback in space coordinates (external disturbances and their balancing occur in space coordinates). Involving the vestibular system in the disturbance estimations facilitates the use of space coordinates in the control [19].

Noticeably, in our approach gravity is considered an external disturbance that is estimated and compensated through sensors. This implies that the control and its input (desired movement signal) are independent of the system’s orientation with respect to the gravity vector. Furthermore, in human balancing, body velocities tend to be low ($< 80^\circ/\text{s}$) so that the balancing is ‘quasi-static’, meaning that Coriolis and centrifugal forces need not be considered.

A major aspect in our extension of the DEC concept to the DIP biomechanics is the handling of inter-link torques in the control.

3 DOUBLE INVERTED PENDULUM MODEL AND ITS CONTROL

The human biomechanics model in terms of a DIP is shown in simplified form in Fig. (2A). The upper segment is given by the trunk (including head and arms) and the lower segment by the legs (excluding the feet). The upper inter-segment joint is the hip joint. The legs are connected to the feet through the ankle joint. In Fig. (2B), COM_T is the center of mass of the trunk and COM_L of the legs, with l giving segment length and h COM height. Angles are defined in Fig. (2C) as trunk-leg angle α_{TL} , trunk-space angle α_{TS} , and leg-space angle α_{LS} . Furthermore, a body-space angle α_{BS} is defined by the line between ankle joint and whole-body COM_B with respect to the space vertical (sv). In the following, uppercase letters in the angle subscripts indicate physical angles and lowercase letters internal representations of these angles.

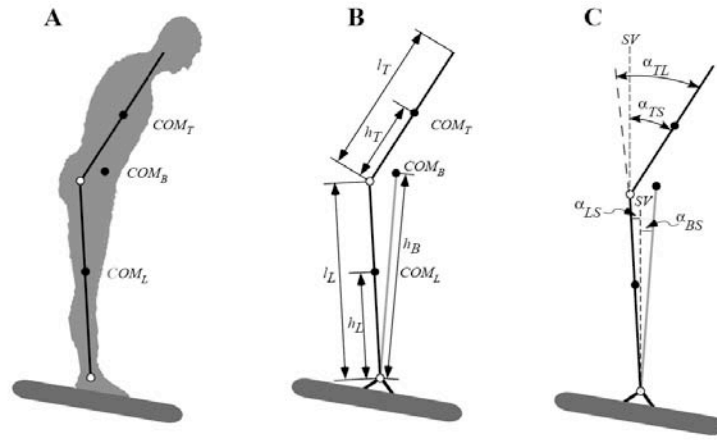


Figure 2: Human double inverted pendulum (DIP) model (A), length parameters of links and COM heights (B), and angles (C). All angles are referenced to fully erect body (0°).

With these simplifications, we used the DIP dynamics elaborated by [20]. Aiming at a sensory feedback control of the DIP, we will try to estimate in addition to the above external disturbances also the inter-link torques through proprioceptive and vestibular sensor signals.

The vestibular system is located on top of the trunk segment (head) and measures trunk angular velocity, attitude and translational acceleration. The vestibular information can be used for the control of legs and feet through coordinate transformations across joints [21].

DIP balancing requires controlling the torques of the ankle and hip joints.

Ankle joint torque. For situations without external disturbances apart from gravity, the ankle torque T_A required to maintain the body upright is

$$\begin{aligned}
 T_A = & \left(J_L + J_T + m_L h_L^2 + m_T (l_L^2 + h_T^2 + 2l_L h_T) \right) \ddot{\alpha}_{LS} \\
 & + \left(J_T + m_T h_T^2 + m_T l_L h_T \right) \ddot{\alpha}_{TL} \\
 & - \left(m_L g h_L + m_T g l_L + m_T g h_T \right) \alpha_{LS} \\
 & - \left(m_T g h_T \right) \alpha_{TL}
 \end{aligned} \tag{1}$$

where $\ddot{\alpha}$ represents angular acceleration, g the gravitational acceleration, m is mass of segment, and J the moment of inertia around the COM. The first two terms give the inertial torques, the last two terms the gravitational torques (compare subscripts in Fig. 2). The sec-

ond and forth terms, arising from hip rotational acceleration ($\ddot{\alpha}_{TL}$) and rotation (α_{TL}), respectively, represent the inter-link torques.

Hip joint torque. The hip torque T_H is given by

$$\begin{aligned} T_H = & \left(J_T + m_T h_T^2 + m_T l_L h_T \right) \ddot{\alpha}_{LS} \\ & + \left(J_T + m_T h_T^2 \right) \ddot{\alpha}_{TL} \\ & - m_T g h_T \alpha_{LS} \\ & - m_T g h_T \alpha_{TL} \end{aligned} \quad (2)$$

where the first and second terms again represent the inertial components and the third and forth terms the gravitational components. The first and third terms, arising from leg-space rotation, yield the inter-link torques.

Envisaged aim of sensory feedback control in the framework of the DEC concept: The two controls (trunk on leg at hip joint and body on foot at ankle joint) operate independently of each other apart from commonly used sensor signals and estimates. In generalized form, this independence provides modularity of the concept.

3.1 Hip joint control model

The control of the trunk reflects the original DEC control of a SIP, in that the inter-link coupling effects are regarded as external disturbances. They occur upon *passive or active* leg motion at the leg's upper end, the hip, which represents the support base for the trunk. They arise in two forms:

(a) Hip translational acceleration \ddot{x}_H , arising upon leg-foot rotational acceleration as tangential hip acceleration, and upon leg-space translational acceleration. It produces hip torque through trunk inertia ($T_{H,in}$).

(b) Hip rotation, arising upon leg-space rotation (α_{LS}) that tends to be taken along with the trunk through passive hip joint stiffness.

Resulting trunk excursions lead to gravitational hip torque ($T_{H,grav}$). Taken together, these are three of the four aforementioned external disturbances (see 2, DEC model). The fourth disturbance, contact force, will not be considered here.

The disturbances are indicated in the Plant inset of the hip control model that is shown in Fig. 3. It depicts schematically how the disturbances are internally estimated through the vestibular system (VEST) and hip angle proprioception (PROP_H). Therewith, we distinguish between kinematic (I) and kinetic (II) effects in the disturbance compensations. Although representing kinetic quantities, the gravitational and inertial torques are estimated in the model on the basis of kinematic sensor signals.

(i) *Estimate of leg-space (trunk support) tilt, $\hat{\alpha}_{LS}$.* The disturbance is accounted for in the model by feeding a signal α_{ls} from an estimate of leg-space tilt $\hat{\alpha}_{LS}$ into the trunk-leg signal α_{tl} that provides the proprioceptive feedback. This ‘upgrades’ the feedback from local (joint) coordinates into space coordinates. The estimate is obtained from summing a vestibular trunk-space angular velocity signal $\dot{\alpha}_{ls}$ and a proprioceptive trunk-leg angular velocity signal $\dot{\alpha}_{tl}$. Further processing of the estimate includes scaling, thresholding, and mathematical integration (see [18]). Feedback of the resulting trunk-space signal (α'_{ls}) meets a desired trunk-space angle signal α_{ls} ! at the input site (lumped time delay, $\Delta t_{H,2}$).

(ii) *Estimate of hip joint gravitational torque, \hat{T}_{H_grav} .* The estimate of gravitational hip torque \hat{T}_{H_grav} is derived from an estimate of trunk-space angle through the vestibular trunk-space signal α_{ts} . This relates to the two gravitational terms of Eq. (2) in the form

$$T_{H_grav} = -m_T g h_T \alpha_{LS} - m_T g h_T \alpha_{TL}. \quad (3)$$

Using this equation for the internal estimate and substituting α_{tl} by $\alpha_{ts} - \alpha_{ls}$ yields

$$\hat{T}_{H_grav} = m_T g h_T \alpha_{ts}. \quad (4)$$

(iii) *Estimate of trunk support (hip) translational acceleration, $\hat{\ddot{x}}_H$.* This estimate is also derived from vestibular signals. It becomes effective through an estimate of the hip inertial torque \hat{T}_{H_in} . Considering the two inertial terms in Eq. (2), we distinguish between SIP external disturbance and the SIP inertia that is effective when one is moving the trunk actively (second term; taken care of by the controller). To this end, we first combine the two inertial terms of Eq. (2)

$$T_{H_in} = (J_T + m_T h_T^2 + m_T l_L h_T) \ddot{\alpha}_{LS} + (J_T + m_T h_T^2) \ddot{\alpha}_{TL} \quad (5)$$

and then substitute $\ddot{\alpha}_{TL}$ by $\ddot{\alpha}_{TS} - \ddot{\alpha}_{LS}$

$$\begin{aligned} T_{H_in} &= J_T \ddot{\alpha}_{LS} + m_T h_T^2 \ddot{\alpha}_{LS} + m_T l_L h_T \ddot{\alpha}_{LS} + J_T \ddot{\alpha}_{TL} + m_T h_T^2 \ddot{\alpha}_{TL} \\ &= m_T l_L h_T \ddot{\alpha}_{LS} + (J_T + m_T h_T^2) \ddot{\alpha}_{TS}. \end{aligned} \quad (6)$$

In the last equation, the second term represents the inertial torque covered by the hip controller C_H in Fig. 3.

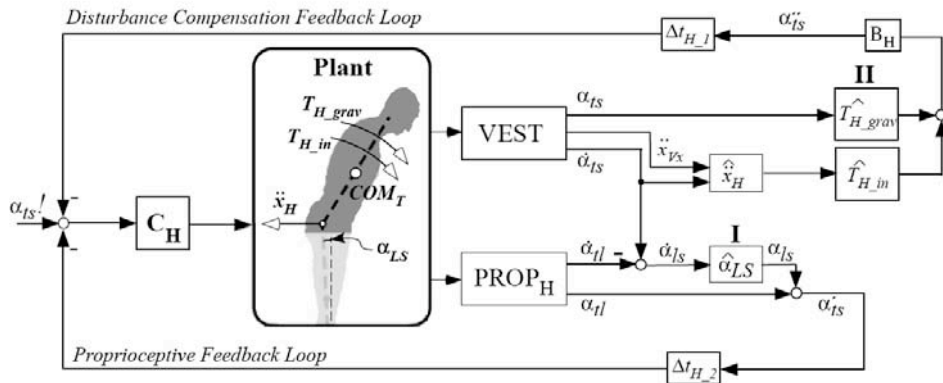


Figure 3: Upper (hip) part of DEC model extended to control DIP biomechanics.

The first term of Eq. (6) represents the torque arising from the hip tangential acceleration \ddot{x}_H . In the DEC concept [18], the estimate of this acceleration, $\hat{\ddot{x}}_H$, is obtained by combining signals of horizontal head (vestibular) translational acceleration \ddot{x}_{Vx} and head angular acceleration (derived from $\dot{\alpha}_{ts}$) in the form

$$\hat{\ddot{x}}_H = \ddot{x}_{Vx} - \frac{d(\dot{\alpha}_{ts})}{dt} l_T. \quad (7)$$

This allows estimating the inertial disturbance torque

$$\hat{T}_{H_in} = -\hat{\dot{x}}_H m_T h_T \cos(\alpha_{ts}) \quad (8)$$

where $\cos(\alpha_{ts}) \approx 1$.

Noticeably, using in Eqs. (7) and (8) sensor signals arising in the trunk (head) implies that also foot support surface translational acceleration is included (not contained in Eq. (2)).

The two torque estimates (ii, iii) are then combined and converted into a signal equivalent to an angular COM_T excursion ('angle equivalent') α''_{ts} in the form of

$$\alpha''_{ts} = \arcsin\left(\frac{\hat{T}_{H_grav} + \hat{T}_{H_in}}{m_T g h_T}\right) \quad (9)$$

(see box B_H in Fig. 3). This is then used in the disturbance compensation feedback (lumped time delay, Δt_{H_I}). The estimates again include scaling and thresholding (see [18]).

3.2 Ankle joint control model

During balancing, the ankle torque has to cope with the *whole body*. The corresponding ankle control model is depicted in Fig. 4 (it resembles in major aspects the hip control model in Fig. 3). Controlling the whole-body COM, COM_B , means in the DEC concept controlling the ankle joint like a SIP through the body-space angle signal α_{bs} . To be applicable to the DIP, however, COM_B is calculated by combining COM_L and COM_T and taking into account the trunk-space and leg-space angles. Applying trigonometric functions to the internal representations α_{ls} and α_{ts} and using the parameters h_L , l_L , and h_T yields the horizontal and vertical positions of COM_B (COM_{BX} , COM_{BY})

$$COM_{BX} = \frac{m_L}{m_B} h_L \sin \alpha_{ls} + \frac{m_T}{m_B} (l_L + h_T) \sin \alpha_{ts} \quad (10)$$

$$COM_{BY} = \frac{m_L}{m_B} h_L \cos \alpha_{ls} + \frac{m_T}{m_B} (l_L + h_T) \cos \alpha_{ts}. \quad (11)$$

From this, α_{bs} is derived

$$\alpha_{bs} = \tan\left(\frac{COM_{BX}}{COM_{BY}}\right). \quad (12)$$

Transformation of leg-space control into body-space control is used below in the following four disturbance estimations.

(i) *Estimate of foot-space (leg support) tilt, $\hat{\alpha}_{FS}$* . This is achieved using vestibular and proprioceptive velocity signals (Fig. 4, I) in an analogous way as described above for the hip control. The resulting foot-space signal α_{fs} is summed with the leg-foot signal α_{lf} , yielding a leg-space signal α'_{ls} . Then the transformation of α'_{ls} into α_{bs} is performed in the way described by Eqs. (10) – (12).

(ii) *Estimate of ankle joint gravitational torque, \hat{T}_{A_grav}* . It is given by

$$\hat{T}_{A_grav} = \alpha_{bs} m_B g h_B \quad (13)$$

where m_B is whole body mass and h_B is COM_B height above ankle joint. The relation to the two gravitational terms of Eq. (1) is presented in Appendix A.

(iii) *Estimate of foot support translational acceleration*, \hat{x}_{FS} (not shown in Fig. 4). It can be derived from \hat{x}_H (compare Fig. 3), leg-space angular acceleration, and leg length in a way analogous to that described above for \hat{x}_H . The corresponding body inertia is then obtained by taking m_B and h_B into account. Because we did not use translational acceleration of foot support as a stimulus in the present study, this estimate is not considered further here.

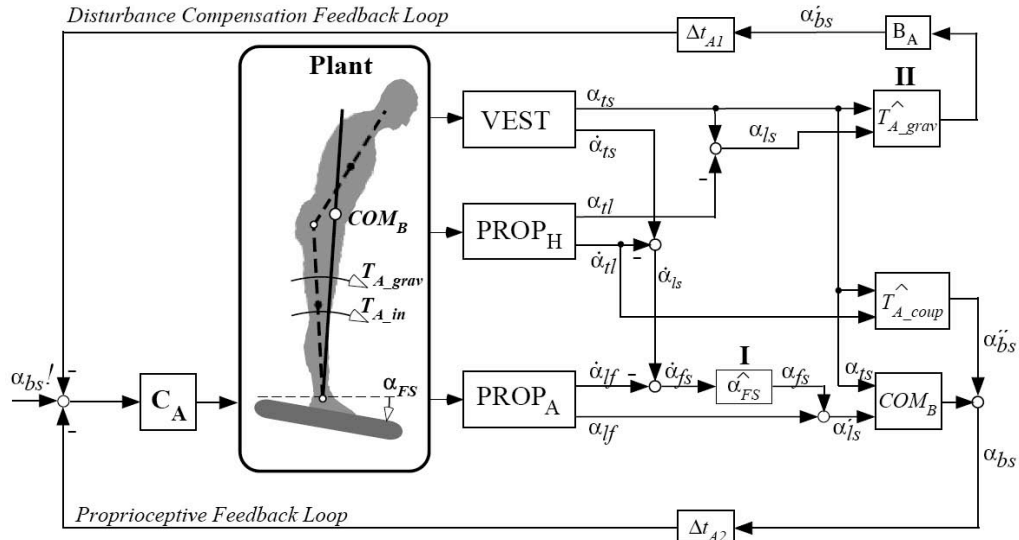


Figure 4: Lower (ankle) part of DEC model extended to control DIP biomechanics.

(iv) *Estimate of ankle joint coupling torque*, \hat{T}_{A_coup} . This inter-link torque arises upon trunk rotational acceleration. It is represented in Eq. (1) by the second term. Ideally (no passive or active joint stiffness, no gravity), the coupling torque T_{A_coup} evokes a passive leg-space counter-motion that is determined by leg and trunk inertia in the form given by the first two terms of Eq. (1). If this motion were completely suppressed (e.g. by the ankle joint control mechanism), the torque would become fully effective and measurable. If, in contrast, the suppression is missing in that the joint control allows for the passive displacement, the passive ankle torque is neutralized. To this end, the control is servoing the displacement equal to an adjustment of its set point signal. This way of inter-link torque compensation is an aspect of the ‘postural adjustment concept’ or ‘movement synergy concept’, according to which humans tend to combine voluntary (pro-active) and reflexive (re-active) trunk-space movements with counter leg-space movements (similar as indicated in the plant inset of Fig. 4; see Discussion). Such a ‘movement synergy’ already results in the DEC concept by stabilizing α_{bs} (see above, *i*, transformation of α'_{ls} into α_{bs}). We asked to what extent the α_{bs} stabilization neutralizes the coupling torque.

Empirically, i.e. in model simulations that included human anthropometric parameters, time delays, passive stiffness and damping, etc. (see below), we found that the leg-space counter-motion evoked by the coupling torque is approximately 20% larger than that evoked already by the body-space control (owing to the fact that body weight fixes the ankle joint on the foot support). Therefore, for a complete neutralization, we explored into an enlargement of the leg counter-motion by using the first two terms of Eq. (1). The ankle joint coupling torque T_{A_coup} is given by the second term of Eq. (1)

$$T_{A_coup} = (J_T + m_T h_T^2 + m_T l_L h_T) \ddot{\alpha}_{TL}. \quad (14)$$

Neutralizing it by a counter leg-space movement requires involving the first term of Eq. (1) in the following form

$$(J_L + J_T + m_L h_L^2 + m_T (l_L^2 + h_T^2 + 2l_L h_T)) \ddot{\alpha}_{LS} = -(J_T + m_T h_T^2 + m_T l_L h_T) \ddot{\alpha}_{TL}. \quad (15)$$

Expressing $\ddot{\alpha}_{LS}$ as a function of $\ddot{\alpha}_{TL}$ (and using internal representations of the physical accelerations) yields

$$\ddot{\alpha}_{LS} = - \left(\frac{J_T + m_T h_T^2 + m_T l_L h_T}{J_L + J_T + m_L h_L^2 + m_T (l_L^2 + h_T^2 + 2l_L h_T)} \right) \ddot{\alpha}_{TL}. \quad (16)$$

In Fig. 4, this estimation is performed within box \hat{T}_{A_coup} , receiving input from $\dot{\alpha}_{tl}$ and α_{ls} . The processing involves a mathematical differentiation of $\dot{\alpha}_{tl}$ and a conversion into \hat{T}_{A_coup} . (This estimate is used in the external contact force estimation, not considered here). For use in the control, $\ddot{\alpha}_{LS}$ is two times integrated, transformed into a body-space angle signal α''_{bs} and then added to the α_{bs} feedback loop.

This procedure tends to neutralize the remaining coupling torque, but does so on the cost of a static COM_B excursion away from its vertical orientation (and of a corresponding COP shift through gravitational torque). We conceived of an alternative solution to compensate the coupling torque by a direct torque feedback or by an indirect one through an angle equivalent (see above, feedback of \hat{T}_{A_grav}). However, we refrained from the latter solutions since their combination with the applied time delays (see below) endangered control stability. In contrast, shifting COM_B through adjustment of the set point signal, as it may occur with voluntary movements or a change in control strategy (e.g. controlling leg-space instead of body-space orientation) did not endanger control stability.

Fusion of hip and ankle joint controls. The two models shown in Figs. (3) and Fig. (4), respectively, were assembled in one model with a hip part and an ankle part such that both shared the VEST and PROP_H sensors. Furthermore, the α'_{ls} signal of the ankle control is ‘up channeled’ for use in the hip control where it replaces the α_{ls} signal (compare [21]).

4 EXPERIMENTAL RESULTS

For testing our control model and comparing it to human and robot data, we applied support surface tilt as disturbance stimulus. A 8° peak-to-peak pseudo-random ternary sequence (PRTS) stimulus was used (see [3]). This stimulus is shown in Fig. 5 together with a representative example of COM_B excursions of a human subject. In the following, gain of the excursions, phase, and coherence are plotted over stimulus frequency (0.016 – 2.2 Hz). Data processing comprised a spectral analysis of the tilt stimuli versus leg-space, trunk-space, and COM_B -space angular excursions and COP shifts using a discrete Fourier transform. In the results (compare e.g. Fig. 6B), zero gain of COM_B would mean that its angular excursion is zero and a gain of unity would mean that it is fully taken along with the tilt. A phase of 0° would mean that its motion is in phase with the stimulus.

4.1 Model simulation

Modeling and simulations were performed in MATLAB/Simulink (The MathWorks Inc., Natick, MA, USA). Anthropometric parameters for our human subjects were calculated ac-

ording to [22]. Control parameters were taken from our previous studies on humans with eyes closed (scaling of disturbance estimates were 0.8, i.e. smaller than ideal = 1; see Appendix B).

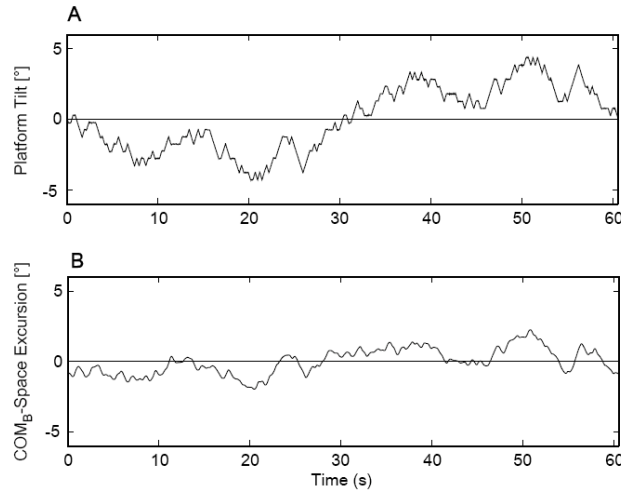


Figure 5: **A** Support surface tilt stimulus. **B** COM_B excursions of a subject. Average of the last five of six stimulus repetitions of one trial.

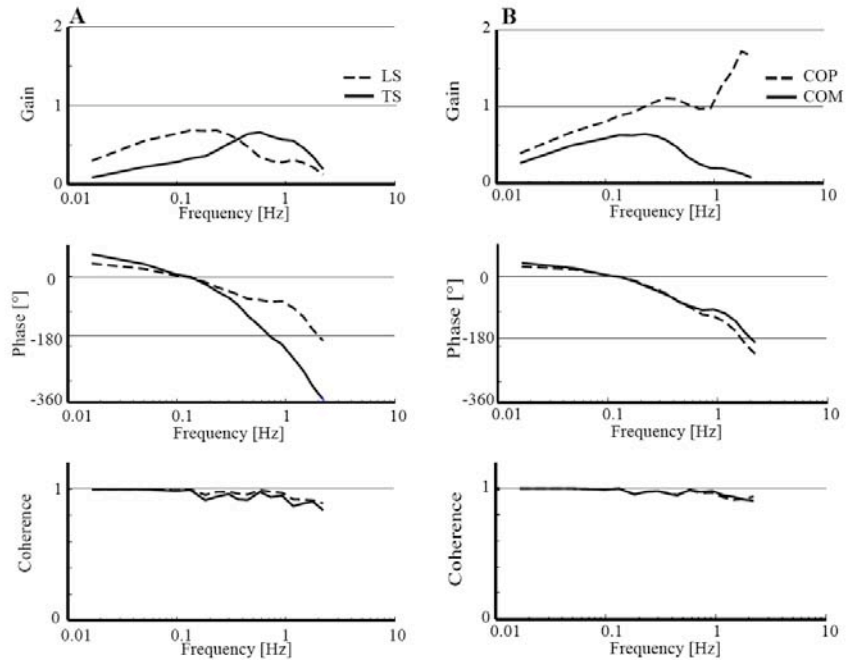


Figure 6: Model simulation. **A** Leg-space (LS) and trunk-space (TS) angular excursion responses evoked by support surface tilt (PRTS stimulus) in terms of gain, phase, and coherence as a function of stimulus frequency. **B** Corresponding responses of COM_B and COP. Gain of LS, TS, and COM_B has no dimension (response [°] / stimulus [°]), whereas COP gain is in $cm/^\circ$ (scaling factor 1.7).

The model simulation results are shown in Fig. 6. With the control parameters used, the tilt stimuli are clearly under-compensated (compare also response curve in Fig. 5). In the following, we describe the main characteristics. Leg-space (LS; Fig. 6A) gain varies with stimulus frequency, showing a maximum at approximately 0.15 Hz and lower values above 0.2 Hz and below 0.1 Hz. In the low frequency range, LS is approximately in phase with the stimulus. With increasing frequency it continuously develops a phase lag. Trunk-space (TS) gain at fre-

frequencies below 0.15 Hz is lower than LS gain (meaning that trunk orientation is more vertical), while the phase develops a similar lag. At 0.15 Hz, there is a cross over of the two gain curves in that TS gain increases and crosses the decreasing LS curve. TS phase lag exceeds more and more the LS phase lag, so that the two curves get approximately into counter phase to each other at 1 Hz and above.

The COM_B gain and phase curves (Fig. 6B) closely resembled those of LS, meaning that the effects of hip joint motion on COM_B are relatively small. The COP gain curves rises with increasing stimulus frequency, this clearly more than the COM_B gain curve, meaning that the ankle torque (relative to tilt amplitude) strongly increases with frequency. Coherence curves of LS, TS, COM_B and COP are almost unity at frequencies below 0.1 Hz, meaning that in the simulations the system behaves approximately linear and without noise. In contrast, the coherence curves fall slightly below unity at the higher frequencies, mainly due to a position threshold in the gravitational torque compensations.

4.2 Human experimental data

Six healthy young subjects (5 male, 1 female) aged 28-35 yrs (mean 30 ± 2.7 yrs) gave their informed consent to the study that was approved by our university's ethics committee. The experiments were performed in the posturographic laboratory of our clinic. Subjects were standing with eyes closed on a 6D servo-controlled motion platform and were presented with the PRTS tilts in the sagittal plane (rotations about ankle joints; for details, see [16]). Instruction was to stand upright. Ears were plugged to reduce auditory orientation cues. LS and TS angular excursions were recorded using an optoelectronic device (Optotrak 3020; Northern Digital Inc.; Waterloo, Canada). COM_B excursions were calculated thereof using the anthropometric parameters given in Tab. 1. COP anterior-posterior shifts were recorded using a force transducing platform (Kistler, Platform type 9286; Winterthur, Switzerland) fixed on the motion platform. Each subject performed the experiment twice.

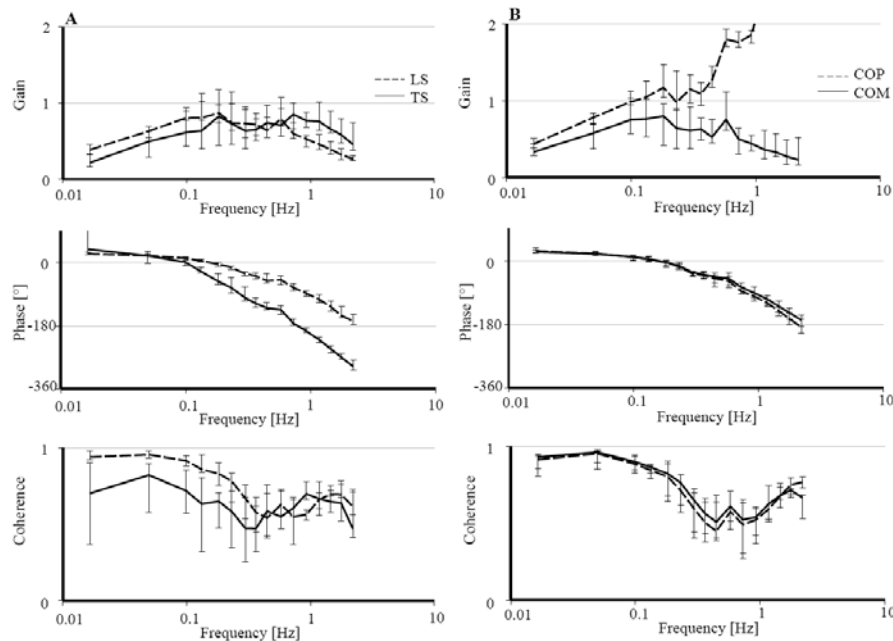


Figure 7: Human experimental data. **A** Gain, phase, and coherence of leg-space (LS) and trunk-space (TS) excursions as a function of tilt stimulus frequency. **B** Corresponding data of COM_B and COP. Median values and 95% confidence intervals. Presentation otherwise as in Fig. 6.

The results are shown in Fig. 7. The main characteristics of the gain and phase curves resemble those of the software simulation in Fig. 6. Note considerable response variability, especially in the mid-frequency range. It stems mainly from inter-subject idiosyncrasies (the individual values already represent averages, taking the last 5 of 6 stimulus repetitions per trial). Inter-subject differences stem mainly from gain rather than phase differences. Interestingly, even larger excursion gains and variations were observed in elderly subjects (not shown), meaning that the system is stable enough to allow even for larger variations in control parameters. Coherence is especially low at frequencies above 0.1 Hz (apart from TS that showed rather low coherence also at the low frequencies).

4.3 Robot experiments

The extended DEC model was embedded into a biped humanoid robot for stance control simulations. It was constructed with human-like anthropometric parameters (Tab. 1; see also www.uniklinik-freiburg.de/neurologie/live/forschung/sensorfusion/PostuRob.html). The robot's trunk, leg and feet segments consist of aluminum frames interconnected by hip and ankle joints. Signals from mechatronic vestibular, joint angle, and joint torque sensor components (see [19]) were input to, and signals for the actuator control (commanding pneumatic 'muscles'; Festo, Esslingen, Germany; Type MAS20) were output from a real time PC. There, the model parts 'Disturbance Estimations' and 'Controller' were executed as a compiled Simulink model (Real-Time Windows Target; The MathWorks Inc., Natick, MA, USA).

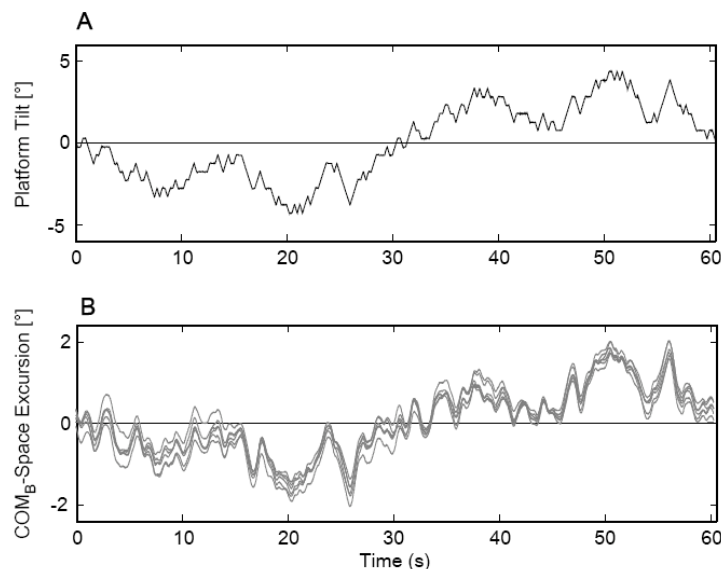


Figure 8: PRTS tilt stimulus (A) evoking COM_B responses in robot (B; ordinate scaling is expanded). Note variability of responses across six stimulus repetitions.

The robot was freely standing on the motion platform and the same experimental procedures as in the human subjects were applied. It showed spontaneous sway, reminiscent to that of humans. Also the responses to the PRTS tilts showed considerable variations (Fig. 8). The gain, phase, and coherence plots are given in Fig. 9. The main characteristics resemble again those obtained in the model simulations (Fig. 6) and the human experiments (Fig. 7). Interestingly, TS coherence at the low frequencies is considerably lower than that of LS, which is similar to the human finding and differs from the model simulation results. A video showing the robot responding to the PRTS tilt can be obtained from the above given web address.

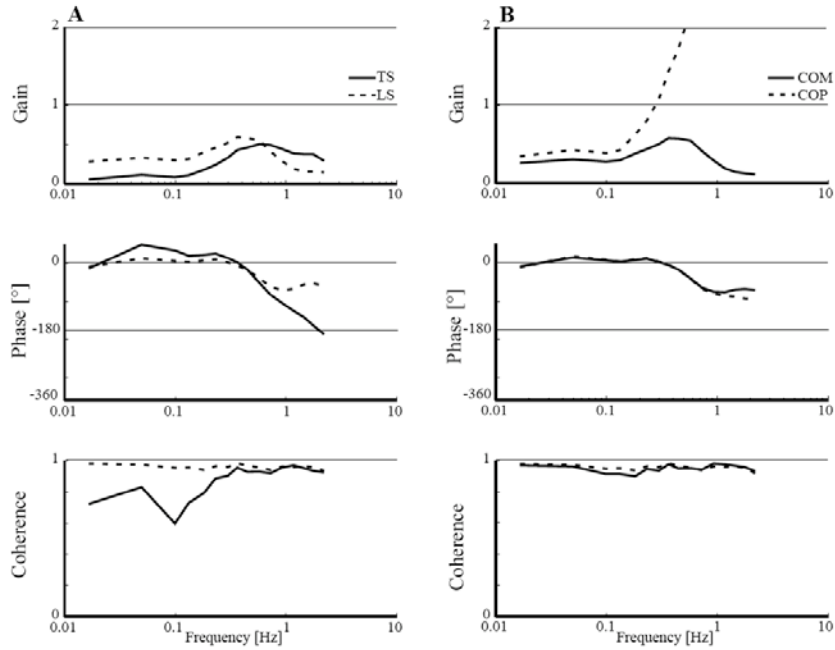


Figure 9: Robot experimental data. **A** Gain, phase, and coherence of LS and TS as a function of tilt stimulus frequency. **B** Corresponding COM and COP results. Presentation as in Fig. 6.

5 DISCUSSION AND CONCLUSIONS

Our study demonstrates that the DEC concept lends itself well to the control of the DIP biomechanics of human biped balancing. The issue has two aspects. First, the DEC concept principally treats the inter-link torques as to-be compensated disturbances, so that these do not hamper higher centers in realizing desired voluntary postures and movements. Second, at the ankle joint, the DEC concept controls body-space orientation, thereby preventing that COP is shifted off its base of foot support. Extending here the concept from SIP to DIP biomechanics entails that changes of COM location within the body in the wake of trunk-leg movements are taken into account.

Concerning the compensation of inter-link torques, the original DEC concept already provided the solutions for the two kinds of hip torques arising upon leg movements (hip torque upon tangential and translational accelerations, estimated and compensated by the estimate \hat{x}_H ; hip torque upon hip rotation through passive joint stiffness and viscosity from joint connective tissues, muscles, etc., accounted for by the estimate $\hat{\alpha}_{LS}$). The solution for compensating the ankle torque arising from trunk movements mainly came with the ankle joint control of α_{BS} (and thereby COM_B) where the trunk movement is combined with a simultaneous counter-rotation of the leg segment. Thereby approximately 80% of this coupling torque is neutralized (in a DIP model with human-like anthropometric parameters). The remaining 20% were estimated by \hat{T}_{A_coup} and could be either removed by increasing the leg counter-rotation such that the neutralization always covers 100% or by counteracting the force directly, thus trying to prevent COM_B motion (a compensation, as it is performed in the full DEC model to counteract, for example, a contact force stimulus such as a push against the body). Currently, our human experimental data does not allow us to decide for one or the other solution (or a more general solution in terms of a flexibility that allows compromises, idiosyncrasies, or task dependent strategies).

Previous studies found that lawful synergies between trunk and leg movements, which minimize the inter-link torques, occur not only during pro-active movements (voluntary hip bending [6,12]), but similarly also during re-active movements (leg and trunk excursions upon foot support surface acceleration [23]). This similarity may suggest that the synergies are generated somewhere down stream in the sensorimotor mechanism. In fact, the authors of the previous studies assume that they are implemented at controller level. Here we show an alternative where the compensation of the inter-link torques emerges from the DEC concept with its inter-sensory interactions. At this point, we would like to point out that the DEC solution is able to incorporate ‘feed forward’ aspects such as changes in response policy (strategy) and prediction [18].

Generally, the compensation of inter-link torques is interwoven in a complex network of factors and constraints so that the identification of the human compensation mechanisms is difficult. For example, using very strong disturbance stimuli that bring biomechanical aspects into the foreground is not a solution that allows general conclusions. In the present study, we recorded human response patterns upon tilt stimuli across a broad range of stimulus frequencies and compared them to corresponding software and hardware-in-the-loop simulations using our DEC concept (see stimulus frequency characteristics in Figs. 6, 7, and 9). These data may in future be complemented by using, in addition, different sets of stimulus amplitudes, disturbance scenarios, voluntary movements, etc. until a rather broad database of the describing and predictive power of a control concept is obtained. Then, a comparison to other control concepts becomes worthwhile.

The robustness aspect was quite evident in our model simulations. Applying in the simulations a previously identified set of control parameters, the tilts were clearly under-compensated. In this form, the simulation data resembled the human data (noticeably, when using ideal parameters, simulated compensation was almost ideal). It is worth to mention that the compensation in humans improves considerably when tested with eyes open (data not shown). The additional visual information, conceivably, improves imperfections in sensory signals and disturbance estimations caused by sensor inaccuracies and noise. Our findings show that the DEC concept tolerates such imperfections. This notion was confirmed in the robot experiments that were performed in the human testbed and faced inaccurate and noisy sensor signals.

In conclusion, we show that the DEC concept lends itself to control the DIP biomechanics of biped disturbance balancing in a human-like way. This suggests modularity in the sense that one can extend the control to further segments. By human-like we mean that it mimics the main characteristics of tilt responses across a broad range of stimulus frequencies, showing robustness against sensor imperfections.

REFERENCES

- [1] D. A. Winter, A. E. Patla, F. Prince, M. Ishac. Stiffness control of balance in quiet standing. *Journal of Neurophysiology*, **80**, 1211–1221, 1998.
- [2] P.G. Morasso, M. Schieppati. Can muscle stiffness alone stabilize upright standing? *Journal of Neurophysiology*, **82**, 1622–1626, 1999.
- [3] R. J. Peterka. Sensorimotor integration in human postural control. *Journal of Neurophysiology*, **88**, 1097–1118, 2002.

- [4] L. M. Nashner, G. McCollum. The organization of human postural movements: a formal basis and experimental synthesis. *Behavioral and Brain Sciences*, **8**, 135-172, 1985.
- [5] L. M. Nashner, F. B. Horak. Central programming of postural movements: adaptation to altered support-surface configurations. *Journal of Neurophysiology*, **55**, 1369–1381, 1986.
- [6] A.V. Alexandrov, A. A. Frolov, J. Massion. Biomechanical analysis of movement strategies in human forward trunk bending. II. Experimental study. *Biological Cybernetics* **84**, 435-443, 2001.
- [7] A. D. Kuo. F. E. Zajac. Human standing posture: Multi-joint movement strategies based on biomechanical constraints. *Progress in Brain Research*, **97**, 349-358, 1993.
- [8] H.C. Diener, F. B. Horak, L. M. Nashner. Influence of stimulus parameters on human postural responses. *Journal of Neurophysiology*, **59**, 1888–1905, 1988.
- [9] J. H. J. Allum, F. Honegger, C. R. Pfaltz. The role of stretch and vestibulo-spinal reflexes in the generation of human equilibrating reactions. *Progress in Brain Research*, **80**, 399-409, 1989.
- [10] F. B. Horak, J. M. Macpherson. Postural orientation and equilibrium. Rowell, L., & Shepherd, J., *Handbook of physiology*. Vol. 1. New York: Oxford University Press. 1996.
- [11] A. D. Kuo, F. E. Zajac. A biomechanical analysis of muscle strength as a limiting factor in standing posture. *Journal of Biomechanics*, **26**, 137–150, 1993.
- [12] A. V. Alexandrov, A. A. Frolov. Biomechanical analysis of movement strategies in human forward trunk bending. I. Modeling, *Biological Cybernetics*. **84**, 425-434, 2001.
- [13] H. van der Kooij, R. Jacobs, B. Koopman, F. van der Helm, F. An adaptive model of sensory integration in a dynamic environment applied to human stance control. *Biological Cybernetics*, **84**, 103–115, 2001.
- [14] A. D. Kuo. An optimal state estimation model of sensory integration in human postural balance. *Journal of Neural Engineering*. **2**, 235–249, 2005.
- [15] T. Mergner, C. Maurer, R.J. Peterka. A multisensory posture control model of human upright stance, *Progress in Brain Research*, **142**, 189-201, 2003.
- [16] C. Maurer, T. Mergner, R.J. Peterka. Multisensory control of human upright stance, *Experimental Brain Research*, **171**, 231–250, 2006.
- [17] K. Masani, A. H. Vette, M. R. Popovic. Controlling balance during quiet stance: Proportional and derivative controller generates preceding motor command to body sway position observed in experiments. *Gait and Posture*, **23**, 164–172, 2006.
- [18] T. Mergner. A neurological view on reactive human stance control, *Annual Reviews in Control*, **34**, 177-198, 2010.
- [19] T. Mergner, G. Schweigart, L. Fennell. Vestibular humanoid postural control. *Journal De Physiologie*, **103**, 178–194, 2009.
- [20] M. AlBakri. Development of a Mathematical Model and Simulation Environment for the Postural Robot (PostuRob II), <http://www.uniklinik-freiburg.de/neurologie/live/forschung/sensorfusion/posturob.html>, 2008.

- [21] T. Mergner, W. Huber, W. Becker. Vestibular-neck interaction and transformations of sensory coordinates. *Journal of Vestibular Research*, **7**, 119–135, 1997.
- [22] D. A. Winter. Biomechanics and motor control in human movement. John Wiley and Sons, New York 1990.
- [23] A. V. Alexandrov, A. A. Frolov, F. B. Horak. Feedback equilibrium control during human standing, *Biological Cybernetics*, **93**, 309–322, 2005.

Appendix A.

To compare the gravitational components in Eq. (1) with the estimates of gravitational torque in the DEC concept, \hat{T}_{A_grav} , we substitute α_{TL} in Eq. (1) by $\alpha_{TS} - \alpha_{LS}$

$$\begin{aligned} T_{A_grav} &= -m_L g h_L \alpha_{LS} + m_T g l_L \alpha_{LS} + m_T g h_T \alpha_{LS} - m_T g h_T \alpha_{TL} \\ &= -m_L g h_L \alpha_{LS} - m_T g l_L \alpha_{LS} - m_T g h_T (\alpha_{LS} + \alpha_{TL}) \\ &= -m_L g h_L \alpha_{LS} - m_T l_L \alpha_{LS} - m_T g h_T \alpha_{TS} \end{aligned} \quad (17)$$

and extend Eq. (17) by $(m_B g)$

$$T_{A_grav} = - \left(\frac{m_L}{m_B} h_L \alpha_{LS} + \frac{m_T}{m_B} l_L \alpha_{LS} + \frac{m_T}{m_B} h_T \alpha_{TS} \right) m_B g. \quad (18)$$

To be able to compare Eq. (18) with the sensor-derived gravitational ankle torque estimate (see below Eq. (22)), we resort to Eqs. (10)-(12) and define height h_B as equal to the vertical coordinate of COM_B (COM_{BY}) in its linearized form

$$h_B = COM_{BY} = \frac{m_L}{m_B} h_L + \frac{m_T}{m_B} (l_L + h_T) \quad (19)$$

Using Eq. (12) in linearized form and replacing COM_{BY} by h_B yields

$$\alpha_{BS} = \frac{COM_{BX}}{h_B} \quad (20)$$

and using Eq. (10) in linearized form for COM_{BX} gives for Eq. (20)

$$\alpha_{BS} \cdot h_B = \frac{m_L}{m_B} h_L \alpha_{LS} + \frac{m_T}{m_B} (l_L + h_T) \alpha_{TS}. \quad (21)$$

Comparability to Eq. (18) is facilitated by replacing $\alpha_{BS} \cdot h_B$ in Eq. (13) by Eq. (21) and using the internal representations of the angles

$$\hat{T}_{A_grav} = \left(\frac{m_L}{m_B} h_L \alpha_{LS} + \frac{m_T}{m_B} (l_L + h_T) \alpha_{TS} \right) m_B g. \quad (22)$$

Appendix B

Table 1 gives the anthropometric parameters and the control parameter used. The anthropometric parameters of Winter [22] were adopted for model simulations using body mass and body height values of our subjects. The control parameters were taken from Maurer et al. [16]. For loop gain adjustments with the PRTS tilt stimulus, see [19].

	Subjects	Model	Robot
Body mass m_B [kg]	69	69	48
Leg mass m_L [kg]	22.2	22.2	14
Trunk mass m_T [kg]	46.8	46.8	34
Body height l_B [m]	1.76	1.76	1.44
Leg length l_L [m]	1.01	1.01	0.86
Trunk length l_T [m]	0.75	0.75	0.58
Body COM height h_B [m]	1.02	1.02	0.9
Leg COM height h_L [m]	0.55	0.55	0.43
Trunk COM height h_T [m]	0.27	0.27	0.25
Body moment of inertia J_B [kg m ²]	17.8	17.8	8.3
Leg moment of Inertia J_L [kg m ²]	4.8	4.8	1.1
Trunk moment of Inertia J_T [kg m ²]	6.4	6.4	2.81
Proportional part of ankle controller [Nm rad ⁻¹]		690	480
Derivative part of ankle controller [Nm rad ⁻¹]		230	80
Integral part of ankle controller [Nm rad ⁻¹]		56	15
Proportional part of hip controller [Nm rad ⁻¹]		127	85
Derivative part of hip controller [Nm rad ⁻¹]		25	4
Integral part of hip controller [Nm rad ⁻¹]		12	5
Time delay of α_{bs} signals [s]		0.15	0.08
Time delay of α_{ts} signals [s]		0.07	0.04
Loop Gain of α_{bs} signal		0.8	0.8
Loop Gain of α_{ts} signal		0.8	4*
Gain of \hat{T}_{H_grav} signal		0.8	0.2*
Gain of \hat{T}_{A_grav} signal		0.8	0.8
Gain of $\hat{\alpha}_{LS}$ signal		0.8	1
Gain of $\hat{\alpha}_{FS}$ signal		0.8	1
Threshold of $\hat{\alpha}_{LS}$ signal [rad s ⁻¹]		0.001	0.003
Threshold of $\hat{\alpha}_{FS}$ signal [rad s ⁻¹]		0.001	0.003
Threshold of \hat{T}_{H_grav} signal [rad]		0.001	0.003
Threshold of \hat{T}_{A_grav} signal [rad]		0.001	0.003

Table 1: Human anthropometric, model simulation and robot simulation parameters. * Adjustments due to technical constraints

Erratum and Comments after publication

Acknowledgements: We like to thank Nicole Gehring and Karim Tahboub for their valuable comments.

Erratum

Page 3, line 4 from below: '>80' changed to '<80'.

Comments

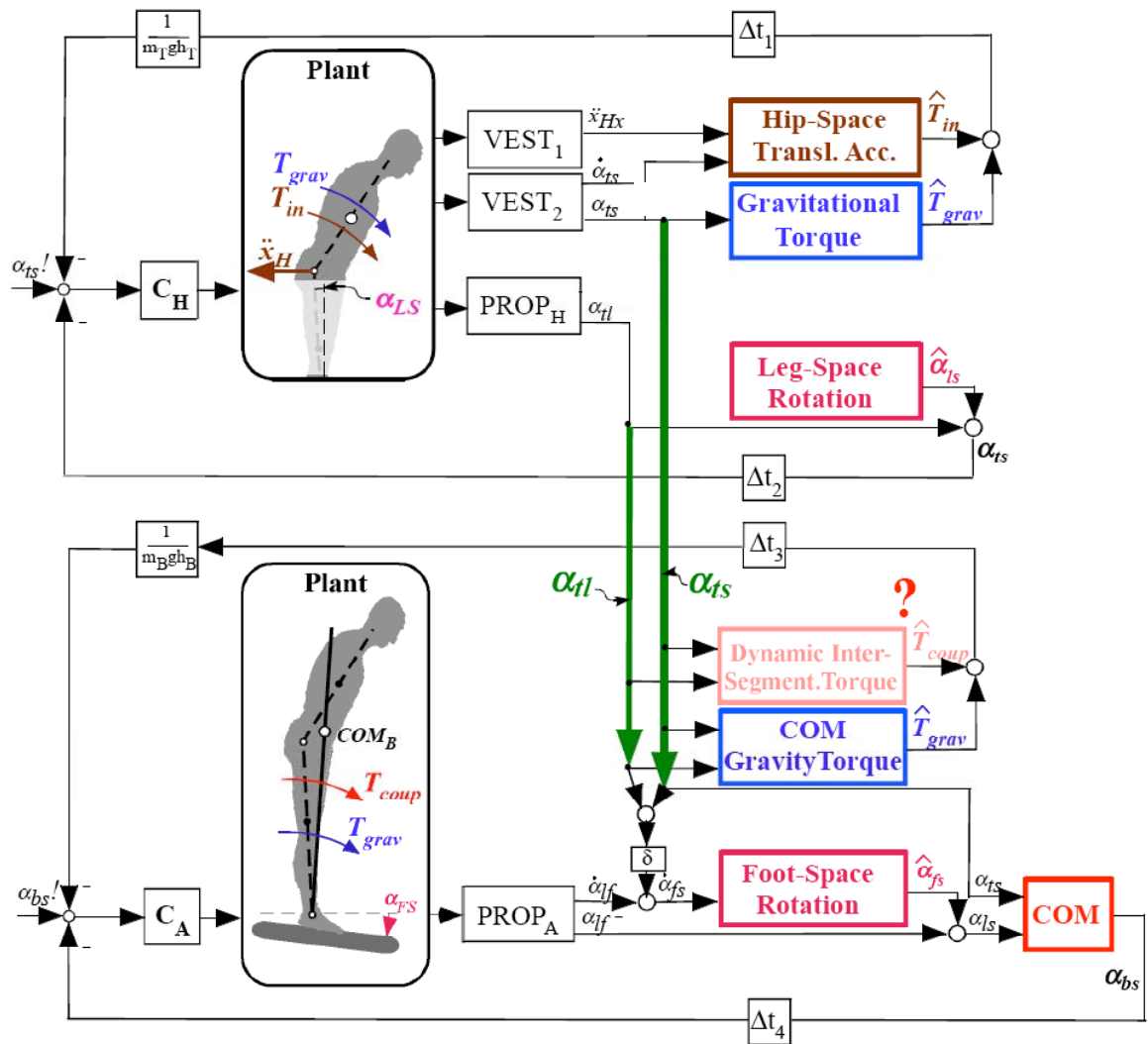
Note that the signs in the above equations that related to the *estimates* of the physical variables changed when considered in relation to the physical variables themselves. Compare, for example, Equ. 4 to Equ. 3. In these equations, furthermore, the small angle simplification was used (the linearized form was also used elsewhere, e.g. page 7, line 3).

In Table 1, the indicated 'adjustments due to technical constraints' meanwhile became superfluous after revising the height of COM of the trunk above the hip joint and the trunk moment of inertia to come closer to human anthropometric values.

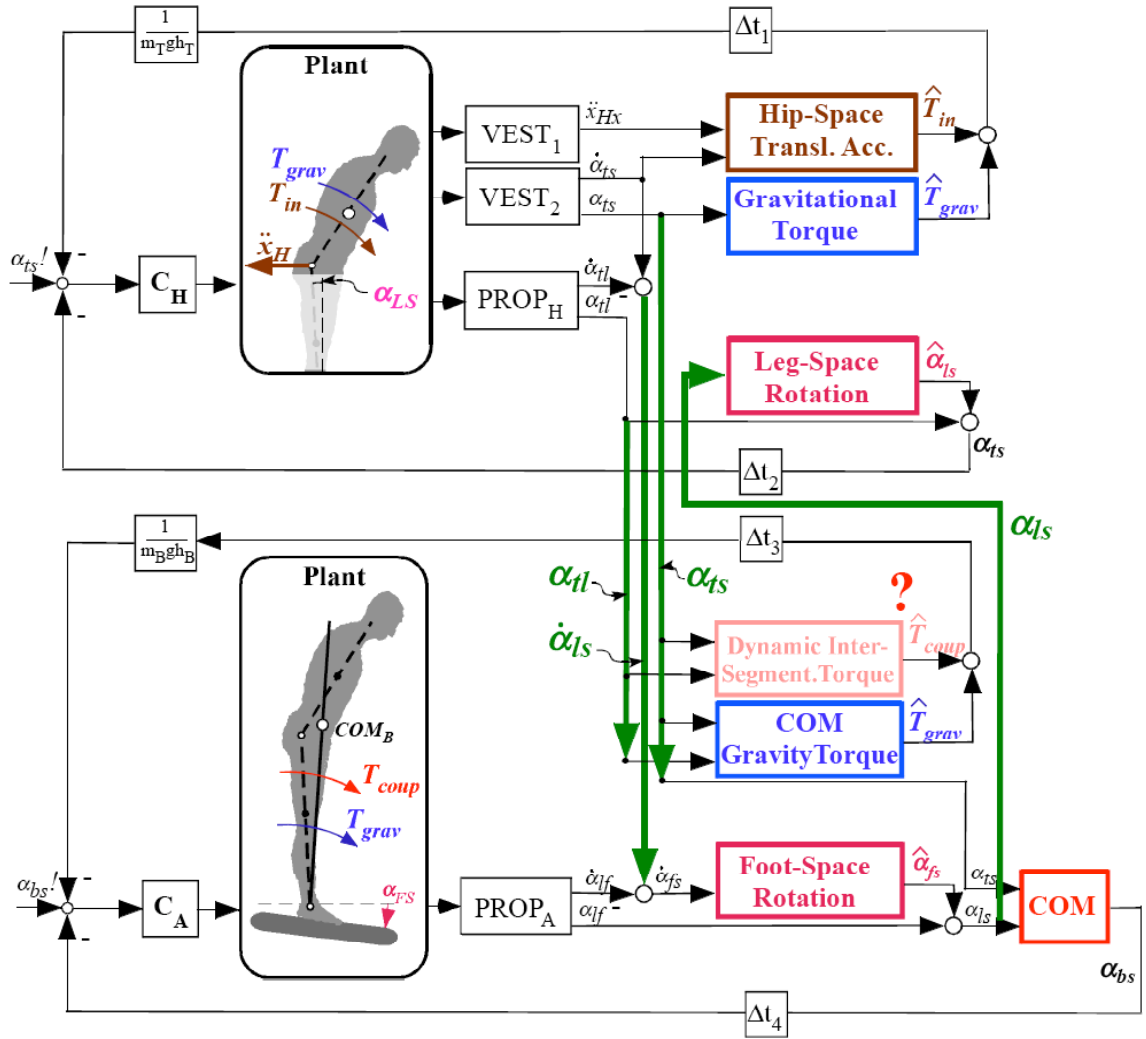
The revised values are: Trunk mass, $m_T = 38$ kg; trunk COM height $h_T = 0.3$ m, trunk moment of inertia, $J_T = 3.2$ kg m²; body mass, $m_B = 52$ kg; body COM height, $h_B = 0.98$ m; body moment of inertia, $J_B = 9.4$ kg m². This revision allowed us to use in the robot the same value (0.8, compare Table 1) as in the model simulations for both the 'Loop Gain of α_{ts} signal' and the 'Gain of \hat{T}_{H_grav} signal'.

In engineering approaches, one may tend to take care of the inter-segmental coupling forces by feeding back in some form the proprioceptive (state) position and velocity signals of one joint to the respective other joint (compare MIMO, multiple inputs- multiple outputs, control system). This we intend to do in future for comparison with the work presented here. Our present approach specifically aimed to test how the DEC concept lends itself to the DIP control problem under the constraint to keep the whole-body COM over the base of its support, making use of the vestibular sensor and its sensory fusions with the proprioceptive sensor (motivations for the multisensory integration concept of the DEC concept, see [18]).

It would be desirable to depict the combination of the above hip joint and ankle joint controls (Figs. 3 and 4, respectively) in one wiring diagram figure to point out their interconnections within the DEC framework. In the above paper, we had not enough space to do so, but presented in our oral talk two versions of such a figure. We add those below. The descriptions are given in the figure legends.



Additional Figure 1: Combining ankle and hip torque controls in one wiring diagram (1st version, model simulation). Note that for the model simulation it sufficed to ‘down channel’ two signals, a proprioceptive trunk-leg signal and a vestibular trunk-space signal. Question mark indicates that omitting the box ‘Dynamic Inter-Segment. Torque’ yielded no considerable changes of simulation results. Presentations are mathematically equivalent to those in Figs. 3 and 4.



Additional Figure 2: Combining ankle and hip torque controls in one wiring diagram (2nd version, robot simulations). The noise of the vestibular sensor (noise color: pink) is considerably larger than that of the proprioceptive sensor. This applies not only to humans, but also to the robot. There, it becomes relevant that the DEC concept uses for the estimate of foot-space rotation a down-channeling of a combination of vestibular and proprioceptive velocity signals (for an effect of a velocity threshold, hidden in the box, on pink noise of the estimate, see [19]). Whenever the robot stands on stationary support, the combination and thus the estimate of foot-space angular motion is zero. As a result, the leg-space feedback signal of the ankle control is determined by the low-noise leg-foot proprioceptive signal alone. Furthermore, by using in addition an ‘up-channeling’ of the leg-space signal, also the ankle joint control profits from the low-noise input. Presentation as in Additional Fig. 1.